ARTICLE

Experimental Research on Mercury Catalytic Oxidation over Ce Modified SCR Catalyst

Yadi Qin, Qiyu Weng and Yuqun Zhuo[*]

Key Laboratory for Thermal Science and Power Engineering of the Ministry of Education, Department of Energy and Power Engineering, Tsinghua University, Beijing, 100084, China

[*]Corresponding Author: Yuqun Zhuo. Email: zhuoyq@mail.tsinghua.edu.cn

ABSTRACT

In order to improve the ability of SCR catalyst to catalyze the oxidation of gaseous elemental mercury, a series of novel Ce modified SCR (Selection Catalytic Reduction, V_2O_5–WO_3/TiO_2) catalysts were prepared via two-step ultrasonic impregnation method. The performance of Ce/SCR catalysts on Hg^0 oxidation and NO reduction as well as the catalytic mechanism on Hg^0 oxidation was also studied. The XRD, BET measurements and XPS were used to characterize the catalysts. The results showed that the pore volume and pore size of catalyst was reduced by Ce doping, and the specific surface area decreased with the increase of Ce content in catalyst. The performance on Hg^0 oxidation was promoted by the introduction of CeO_2.Ce_1/SCR (1%Ce, wt.%) catalyst exhibited the best Hg^0 oxidation activity of 21.2% higher than that of SCR catalyst at 350°C, of which the NO conversion efficiency was also higher at 200–400°C. Furthermore, Ce_1/SCR showed a better H_2O resistance but a slightly weaker SO_2 resistance than SCR catalyst. The chemisorbed oxygen and weak absorbed oxygen on the surface of catalyst were increased by the addition of CeO_2. The chemisorbed oxygen and weak absorbed oxygen on the surface of catalyst were increased by the addition of CeO_2. The Ce_1/SCR possed better redox ability compared with SCR catalyst. HCl was the most effective gas responsible for the Hg^0 oxidation, and the redox cycle (V^{4+} + Ce^{4+} ↔ V^{5+} + Ce^{3+}) played an important role in promoting Hg^0 oxidation.

KEYWORDS

Mercury catalytic oxidation; SCR catalyst; Ce doping; reaction mechanism

1 Introduction

Mercury is considered an important environmental pollutant due to its toxic, bioaccumulative and long-distance transport properties. The global mercury emissions reached 6,500 ton/year in 2014, and it will reach 8,600 tons per year in 2035 according to the ECHMERIT model [1]. In 2013, more than 80 countries and regions, including China, signed the Minamata Convention, which sets the binding standards for mercury-containing products and mercury emissions to atmosphere. Data show that over 3,000 tons of mercury from burning coal are emitted per year globally, and more than 90% of mercury from coal-fired power plants is released into the atmosphere [2]. After coal combustion, mercury mainly exists in coal cinder, fly ash and flue gas, and the content is about 2%, 23.1%~26.9% and 56.3%~69.7%, respectively [3]. The average distribution of mercury in flue gas was 56% elemental mercury (Hg^0), 34% bivalent

mercury (Hg^{2+}) and 10% particulate mercury (Hg^P) [4]. Hg^{2+} is soluble and easy to react with limestone, more than 80% of which can be removed by wet limestone-gypsum FGD device [5]. About 90% of Hg^P can be captured by electrostatic precipitator, bag filter and other dust removal equipment [6]. However, the air pollution control device (APCDs) has little effect on Hg^0 removal [7]. After long-term screening, SCR catalyst with the component of V_2O_5–WO_3–TiO_2 is the most widely used in coal-fired power plants. It is found that SCR catalyst can catalyze the conversion of Hg^0 to Hg^{2+}, which can be removed by subsequent dedusting and FGD equipment [8]. However, researches showed that Hg^0 oxidation over SCR catalyst was limited, highly dependent on the concentration of HCl in flue gas with poor water resistance [9].

Doping metal oxides into SCR catalysts to improve the oxidation effect of mercury without decreasing the denitrification efficiency has become the focus of current research. CeO_2 could provide significant oxygen storage capability through the redox shift between the two oxidation states (Ce^{3+} and Ce^{4+}), which is helpful to enhance catalytic activity [10]. It was found that the catalytic activity of Ce/SCR catalyst was higher than that of Fe/SCR, Mn/SCR, Cu/SCR and Co/SCR catalysts [11]. The research of Ce/SCR catalyst is still at the initial stage, the optimal temperature for catalytic performance of Hg^0 oxidation over Ce/SCR catalyst is low due to the large Ce doping amount and the catalyst performs poorly at the normal operating temperature (280°C–420°C) in power plant [12]. Within the operating temperature range of SCR catalyst in power plant, the optimum amount of Ce doping have not been determined at present [11–14]. Some research such as the effect of flue gas and the mechanism on Hg^0 oxidation over Ce modified SCR catalysts also need to be studied.

In this study, a series of CeO_2 modified support on V_2O_5–WO_3/TiO_2 catalysts were made by ultrasonic-assisted impregnation method. The Hg^0 and NO oxidation efficiencies of the catalysts were tested under simulated flue gas. Besides, the effects of individual flue gas components on Hg^0 oxidation were also evaluated. Furthermore, X-ray diffraction (XRD), Brunner−Emmet−Teller (BET) and X-ray photoelectron spectroscopy (XPS) were explored to characterize the catalysts, and the reaction mechanism was discussed based on the experimental and characterization results.

2 Experimental

2.1 Catalyst Preparation

Cerium nitrate which was the precursor of CeO_x will react with ammonium metavanadate precursor or ammonium tungstate precursor to produce cerium vanadate or cerium tungstate precipitation, affecting the uniformity of V_2O_5 and CeO_2 on the surface of TiO_2. Therefore, modified catalysts were prepared by multi-step ultrasonic impregnation method based on the common commercial SCR catalysts (containing 1%V_2O_5, 9%WO_3 and 90%TiO_2). TiO_2 was added into mixed solutions of ammonium metavanadate, ammonium metatungstate and oxalic acid. The slurry was exposed to an ultrasonic bath for 4 h, dried at 105°C for 4 h and calcined at 500°C for 4 h in air to obtain SCR catalyst. $Ce(NO_3)_3$ was dissolved in deionized water at different concentrations. The powder of SCR catalysts was impregnated in $Ce(NO_3)_3$ solution for 4 h, dried at 105°C for 4 h and calcined at 500°C for 4 h. Finally, CeO_2 doped catalyst V_2O_5–WO_3/TiO_2 was obtained and abbreviated as Ce_x/SCR. X represents the mass fraction of Ce in the sample, x = 0.5%, 1%, 3%, 5%. 80–100 mesh particles were selected by stainless steel sieve.

2.2 Catalytic Activity Test

The schematic of the fixed-bed reactor system used for Hg^0 oxidation was showed in Fig. 1. The reactor system consists of four parts: mercury generation, simulated flue gas mixing, temperature control and mercury analysis.The elemental mercury was generated by a PSA Cavkit 10.534 mercury generator. The water vapor was generated by an IAS Hovocal gas generator. The composition and concentration of simulated flue gas were controlled by mass flow controllers (MFCs). The fixed-bed reactor was made of a quartz tube heated in a vertical tubular furnace. The catalyst sample was placed between the quartz cotton

and glass fiber filter membrane, which were loaded in the quartz reactor. The concentrations of Hg^0 and Hg^{2+} in simulated flue gas were online monitored by Thermo CEMS. To avoid Hg contamination, all of the tubes, joints, and valves that Hg passed through were made of Teflon. To avoid condensation of water vapor, all pipelines with H_2O (g)-containing gas passing through were heated up to 120°C. The tail gas was treated by an activated carbon trap before being released to the air.
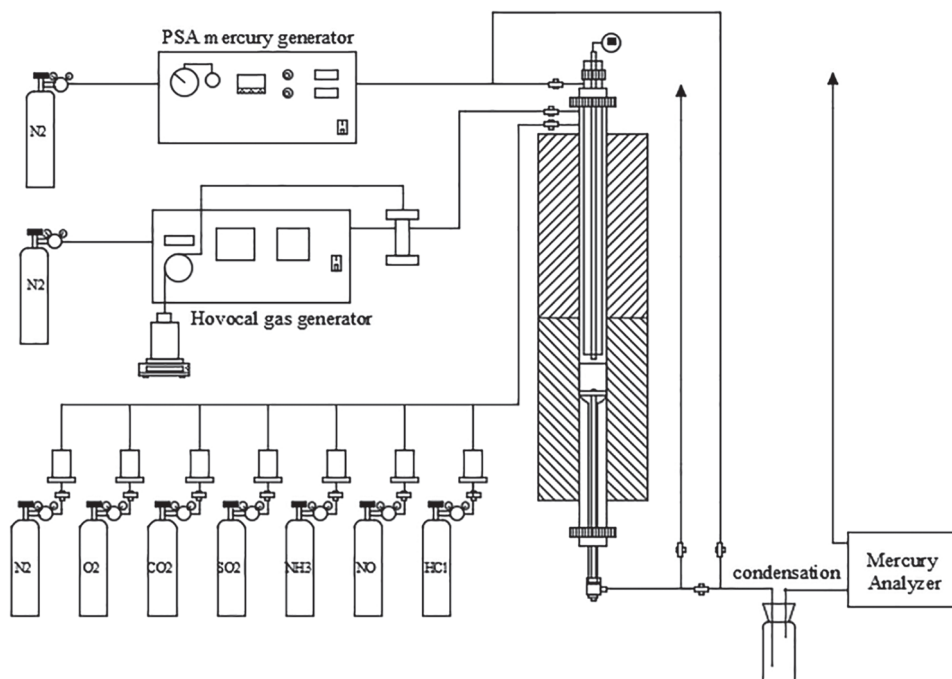
Figure 1: Schematic diagram of experimental system for mercury oxidation

The inlet Hg^0 concentration was set at 30 μg/Nm³ and the total flow rate of simulated flue gas was controlled at 2 L/min. The concentration of Hg^0 and Hg^{2+} at the outlet was recorded after adsorption balance, which was defined as the fluctuation of concentration less than 3%. The time for the balance was more than 2 h. The total Hg^0 oxidation rate (O_{xi}) within a certain time was defined as follows:

$$o_{xi} = \frac{\sum_t^0 \dfrac{C_{Hg^{2+}}^t}{C_{Hg^T}^t}}{t} \tag{1}$$

where $C_{Hg^{2+}}^t$ and $C_{Hg^T}^t$ were the outlet Hg^{2+} and total mercury concentration at the reaction time, respectively.

2.3 Characterization

XRD measurements were carried out on polycrystalline X-ray diffractometer (Smartlab, Rigaku, Japan) to examine the crystallinity and dispersivity of crystal pieces using Cu Ka radiation (9 KW) in the range of 3–90°. The specific surface area, pore volume and pore diameter of catalysts were tested on automatic nitrogen adsorption analyzer (Micrometritics ASAP2010). The surface area and pore size was calculated by Brunauer−Emmett−Teller (BET) method and Barrett−Joyner−Halenda (BJH) method, respectively. To investigate the elemental states, XPS was carried out by X-ray photoelectron spectrometer (PHI QuANTRO SXM, ULVAC-PHI, Japan). The observed spectra were calibrated with the C1s binding energy (BE) value of 284.6 eV.

3 Results and Discussion

3.1 Hg^0 Oxidation Activity over Various Catalysts

Fig. 2 showed the Hg^0 catalytic oxidation efficiencies over various catalysts with a space velocity of 60000 h^{-1} in the temperature range of 150–400°C. The simulated flue gas consisted of 10 ppm HCl, 12% CO_2, 5% H_2, 300 ppm NO, 400 ppm SO_2 and N_2 as balance gas. The results indicated that Ce doping did not change the optimum Hg^0 catalytic oxidation temperature over SCR catalyst, which was still 350°C. It was clearly found that the addition of CeO_2 resulted in enhancement of Hg^0 oxidation activity in varying degrees. With the increase of Ce doping, the Hg^0 oxidation efficiency over Ce_x/SCR catalyst first increased and then decreased at 350°C. Ce_1/SCR performed the best mercury oxidation and approximately 84.24% mercury oxidation efficiency was obtained. It was worth noting that the Hg^0 oxidation rate of Ce_5/SCR decreased remarkably, even less than the Hg^0 oxidation rate of SCR when the temperature exceeded 350°C. It was presumed that CeO_2–TiO_2 performed optimal Hg^0 catalytic oxidation at about 150°C [15], and excessive Ce doping lead to poor Hg^0 oxidation over Ce_5/SCR at high temperature.
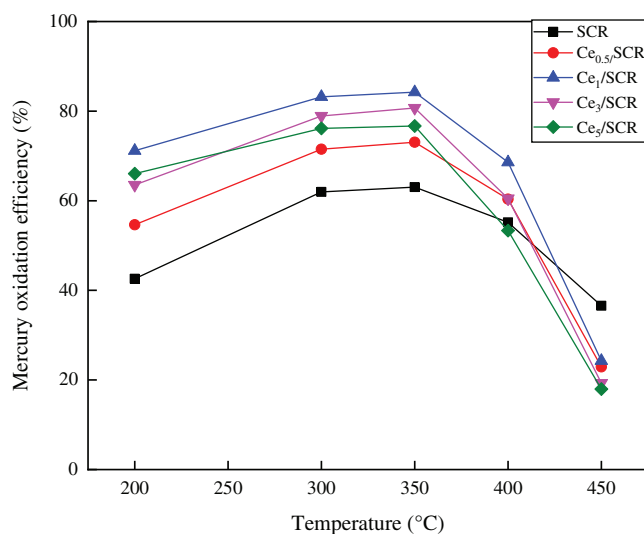
Figure 2: Comparison of catalytic activity for Hg^0 oxidation over Ce_x/SCR catalysts

3.2 Effect of Flue Gas Constituents on Hg^0 Oxidation

3.2.1 Effect of SO_2

The comparison of effect of SO_2 on Hg^0 oxidation efficiency over Ce_1/SCR and SCR catalyst was measured in Fig. 3. The results indicated that SO_2 had a slightly promotional effect on Hg^0 oxidation over SCR catalyst. SO_2 was oxidized by chemisorbed oxygen to form SO_3, which constituted new chemisorption sites for Hg^0 and reacted with Hg^0 to produce $HgSO_4$ [15]. However, SO_2 exhibited a weak inhibiting effect on Ce_1/SCR catalytic activity. This could be due to that SO_2 reacted with Ce_xO_y to form $Ce(SO_4)_2$ and $Ce_2(SO_4)_3$, which reduced the participation of Ce_xO_y in Hg^0 oxidation process and covered the surface of Ce_1/SCR catalyst, reducing the contact area between the active components and the reaction gas. Because Ce content in Ce_1/SCR catalyst was only 1%, SO_2 had no obvious inhibition on Hg^0 oxidation over Ce_1/SCR catalyst.
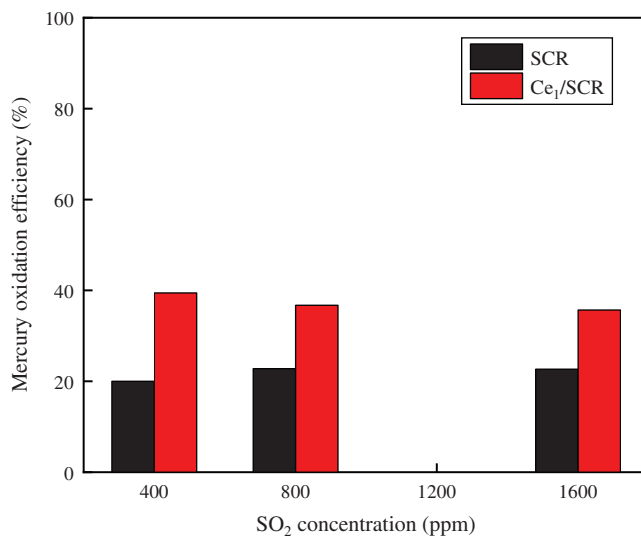
Figure 3: Effect of SO_2 on Hg^0 oxidation over SCR and Ce_1/SCR catalyst at 350°C. Reaction conditions: 0.6 ppm HCl, 5% O_2, N_2 as balance gas

3.2.2 Effect of H_2O

The results that the effect of H_2O on Hg^0 oxidation efficiency over Ce_1/SCR and SCR catalyst was shown in Fig. 4. H_2O inhibited Hg^0 oxidation due to the competitive adsorption between H_2O and Hg^0 [13]. However, Ce_1/SCR catalyst had a superior performance of H_2O resistance than SCR catalyst. It was speculated that the active sites on the surface increased or the adsorption of water vapor decreased by doping Ce into SCR, or the transition between Ce^{4+}/Ce^{3+} was likely to offset part of the inhibitory effect of H_2O.
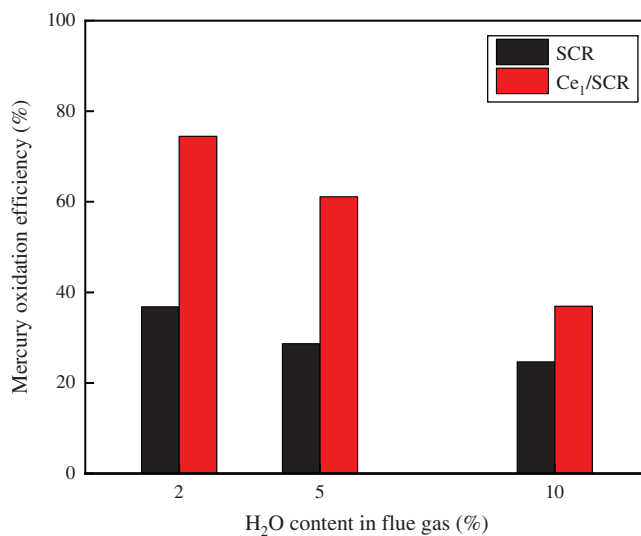
Figure 4: Effect of H_2O on Hg^0 oxidation over SCR and Ce_1/SCR catalyst at 350°C. Reaction conditions: 30 ppm HCl, 5% O_2, N_2 as balance gas, GHSV = 600000 h^{-1}

3.2.3 Effect of NO

Fig. 5 showed the effect of NO on Hg^0 oxidation over Ce_1/SCR catalyst. It indicated that NO had a slight enhancing effect on Hg^0 oxidation. This probably because NO reacted with chemisorbed oxygen to form NO_x species, which could enhance Hg^0 oxidation.
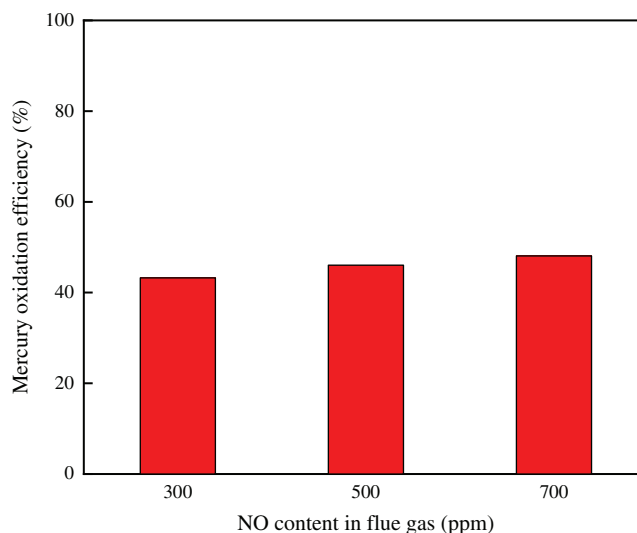
Figure 5: Effect of NO on Hg^0 oxidation over Ce_1/SCR catalyst at 350°C. Reaction conditions: 0.6 ppm HCl, 5% O_2, N_2 as balance gas

3.3 NO Reduction Activity over Various Catalysts

Catalytic activity evaluation was carried out using a flow-through powder reactor system referred in Pang et al. [16]. NO concentration was tested for 30 min at each steady state. The NO conversion was calculated using the equation below:

$$N_{oxi} = \frac{\Delta\overline{NO}}{NO_{in}} = \frac{NO_{in} - \overline{NO_{out}}}{NO_{in}} \tag{2}$$

where NO_{in} represents the inlet NO concentration maintained at 500 ppm and NO_{out} represents the outlet average NO concentration.

The NO conversion over SCR and Ce_1/SCR catalyst at various temperature were showed in Fig. 6. The NO conversion over SCR catalyst was noticeably enhanced by Ce doping. SCR catalyst performed best NO conversion at 400°C while Ce_1/SCR catalyst performed best at 350°C. It was speculated that Ce had a good effect on catalytic oxidation at low temperature, which decreased the optimal denitrification temperature. At operating temperature (300–400°C) of catalyst in power plant, NO conversion over Ce_1/SCR catalyst was greater than 90%, which had a small difference from the optimal denitrification efficiency. Therefore, Ce_1/SCR can be well applied in power plant, which will have a better simultaneous removal performance of NO and Hg^0 than SCR.
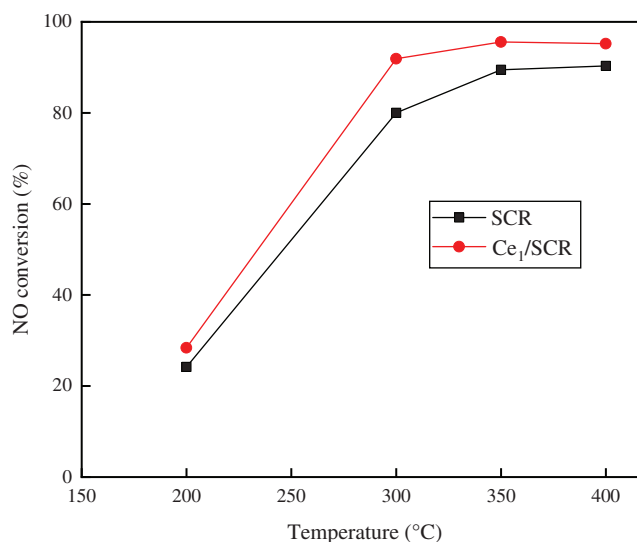
Figure 6: NO conversion over SCR and Ce$_1$/SCR catalyst. Reaction conditions: NO 500 ppm, NH$_3$ 500 ppm, O$_2$ 3%, and SO$_2$ 400 ppm, balance N$_2$, GHSV = 20000 h^{-1}

4 Catalyst Characterization

4.1 XRD

The XRD patterns of the raw and modified SCR catalysts were displayed in Fig. 7. TiO$_2$ phase other than rutile TiO$_2$ phase was detected in all samples. The diffraction line of all samples were narrow and sharp, which indicated the high crystallinity. The characteristic peaks of V$_2$O$_5$ and WO$_3$ were hardly detected, which were due to widely dispersion and poorer crystalline on the surface. CeO$_2$ was not observed when the loading of Ce was lower than 3% (wt.%). There were weak characteristic CeO$_2$ peaks at 28.38° when the loading of Ce was 5%, indicating a well-dispersed cluster with a small population of CeO$_2$ may exist.
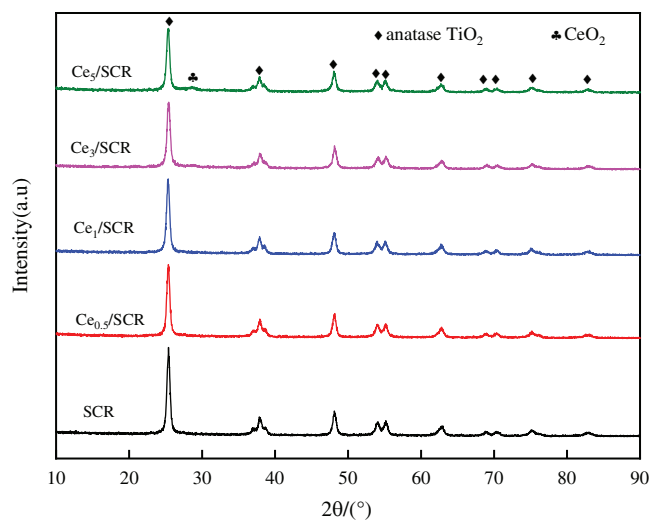
Figure 7: XRD profiles of Ce$_x$/SCR catalysts with different Ce contents

4.2 BET

The pore structure parameters of different samples were summarized in Table 1. As can be seen from the result, the BET surface area, BJH pore volume and average pore volume of Ce_x/SCR catalyst were lower than those of SCR. The BET surface area of Ce_x/SCR decreased with the increase of Ce doping amount. The pore volume and pore diameter of Ce_x/SCR catalyst did not show obvious relationship with Ce doping amount. The Nitrogen adsorption-desorption isotherms of Ce_x/SCR were the IV adsorption-desorption isotherm specified by IUPAC. H1 hysteresis loop indicated mesoporous materials, which might facilitate mass transfer in the catalytic reaction (Fig. 8a). As displayed in Fig. 8b, Ce doping had no significant effect on the pore size distribution of catalysts. There were much mesoporous of 2~50 nm in Ce_x/SCR catalysts, indicating strong interactions between catalyst surface and adsorbate.

Table 1: The specific surface area and crystallite size of the catalysts

Catalysts	BET surface area (m^2/g)	Pore volume (cm^3/g)	Average pore diameter (nm)
SCR	71.9646	0.2907	161.5863
$Ce_{0.5}/SCR$	71.8637	0.2802	155.9777
Ce_1/SCR	71.1684	0.2543	142.9438
Ce_3/SCR	70.6369	0.2727	154.4254
Ce_5/SCR	67.8422	0.2607	153.7143
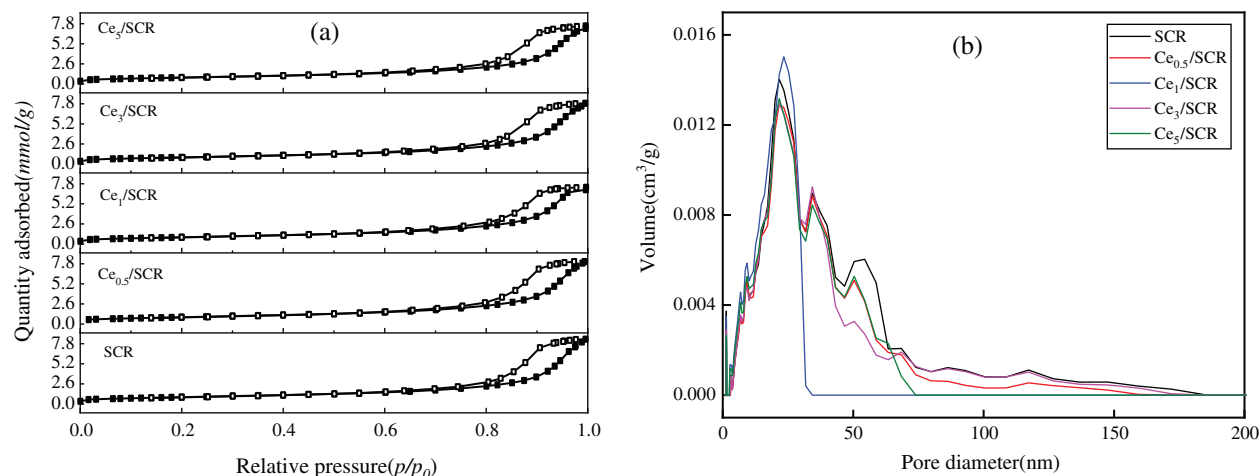
Figure 8: Physical properties of different catalysts. (a) N_2 adsorption and desorption isotherms; (b) Particle size distribution

5 Mechanism

5.1 Hg^0 Oxidation Reaction

The effects of HCl and O_2 on mercury oxidation over Ce_1/SCR catalyst were shown in Fig. 9. Ce_1/SCR catalyst showed less than 5% mercury oxidation efficiency whether 5% O_2 was introduced into gas stream or not. Considering the measurement error, O_2 had little effect on Hg^0 oxidation. That was probably because the level of reaction between O_2 and Hg^0 was low, generating unstable Hg^{2+} which coule convert to Hg^0 easily.

$$2Hg + O_2 \rightleftharpoons 2HgO \tag{3}$$

0.1 ppm HCl balanced in N_2 resulted in Hg^0 oxidation efficiency of 13.02%, which is higher than the 2.73% Hg^0 oxidation efficiency under pure N_2 condition. Hg^0 oxidation efficiency of 64.68% was observed when HCl concentration further increased to 1 ppm. HCl exhibited a decisive effect on Hg^0 oxidation over Ce_1/SCR catalyst. 0.1 ppm HCl resulted in Hg^0 oxidation efficiency of 50.42% with the aid of 5% O_2, indicating more HCl can be oxidized to form active chlorine species in the presence of O_2. That might because O_2 replenished the consumed chemisorbed oxygen, regenerated the lattice oxygen and hence maintained the high surface oxygen concentration [15]. The reaction between HCl and Ce_1/SCR catalysts may occur through

$$2HCl + O = 2Cl + H_2O \tag{4}$$

$$Cl + Hg^0 = HgCl \tag{5}$$

$$HgCl + Cl = HgCl_2 \tag{6}$$
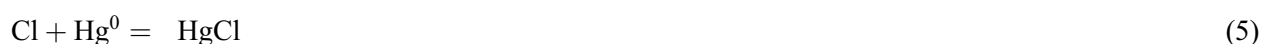
where Cl denoted an active chlorine species for oxidizing Hg^0, and O represented chemisorbed or lattice oxygen on the surface of Ce_1/SCR catalysts.

The entire reaction can be written as follows:

$$Hg^0 + 2HCl + \frac{1}{2}O = HgCl_2 + H_2O \tag{7}$$
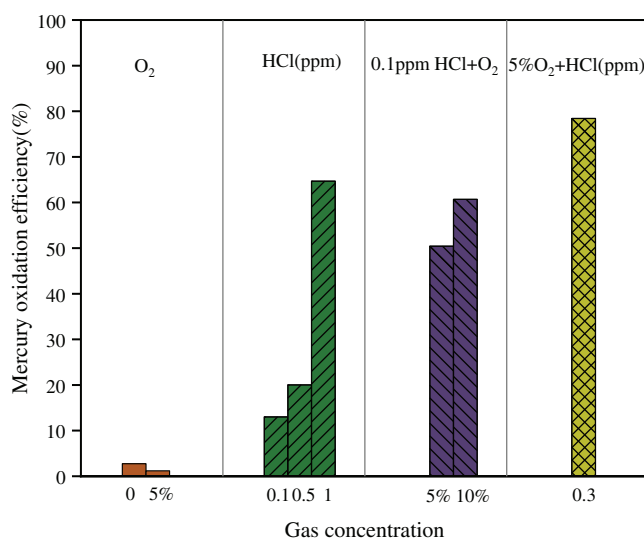
Figure 9: Effects of HCl and O_2 on Hg^0 oxidation of Ce_1/SCR catalyst at 350°C. Reaction conditions: balance N_2, GHSV = 20000 h^{-1}

5.2 XPS

To determine the oxidation states of the element in these catalysts and to further explain the mechanism of Hg^0 oxidation over Ce_1/SCR catalyst, the catalysts were investigated by XPS technique. Ce_1/SCR catalyst was pretreated in the gas composed of 50 μg/m^3, 10 ppm HCl and 5% O_2 at 350°C for 4 h to get sCe_1/SCR catalyst. Fig. 10 showed the O1s XPS spectra for SCR, Ce_1/SCR and sCe_1/SCR catalyst. The peak appeared

at low binding energy (529–530.5 eV) could be ascribed to be the lattice oxygen (denoted as O_b) [17], while the binding energy of 531.0–532.9 eV was ascribed to the chemisorbed oxygen and weakly bonded oxygen species (denoted as O_a) [18]. O_a has been thought to be the most active oxygen and played an important role in oxidation reaction [18–19]. The surface atomic concentrations of catalysts are given in Table 2. It could be found that O_a relative concentration of Ce_1/SCR calculated by $O_a/(O_a + O_b)$ was higher than that of SCR. The reason was that Ce doping created labile oxygen vacancies, which may conduce to the improvement of chemisorbed oxygen and was helpful for mercury oxidation. The Ce3d spectra of sCe_1/SCR and Ce_1/SCR catalysts were presented in Fig. 11. The bands labeled u1 and v1 represent the characteristic peaks of Ce^{3+} with 3d104f1 initial electronic state, whereas the peaks labeled u, u2, u3, v, v2, and v3 represent Ce^{4+} with 3d104f0 electronic state [20].
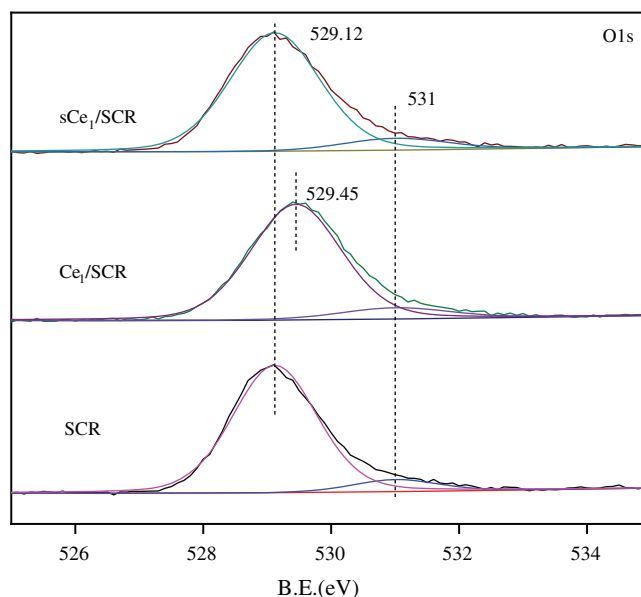
Figure 10: O1s XPS spectra for SCR,Ce_1/SCR and Ce_1/SCR

Table 2: Results of quantitative XPS analysis

Samples	$O_\alpha/(O_\alpha + O_\beta)$	$Ce^{3+}/(Ce^{3+} + Ce^{4+})$
SCR	8.64%	
Ce_1/SCR	10.61%	33.66%
sCe_1/SCR	10.48%	29.98%

Table 2 showed a slight change in the Ce valence state ratios after the tests under a flue gas flow. This implied that the redox shift between Ce^{3+} and Ce^{4+} happened during the Hg^0 catalytic oxidation process. In comparison with Ce_1/SCR, the relative concentration of Ce^{3+} species decreased in sCe_1/SCR, which might be due to sufficient O_2 in flue gas to oxidize Ce^{3+} to Ce^{4+}.

The Hg4f XPS profile spectrum of sCe_1/SCR catalyst was presented in Fig. 12. The binding energies at 101.5 and 110.5 eV was corresponded to $HgCl_2$ and HgO, respectively. No Hg^0 was observed on the surface of sCe_1/SCR catalyst, which probably because HCl accelerated Hg^0 oxidation.
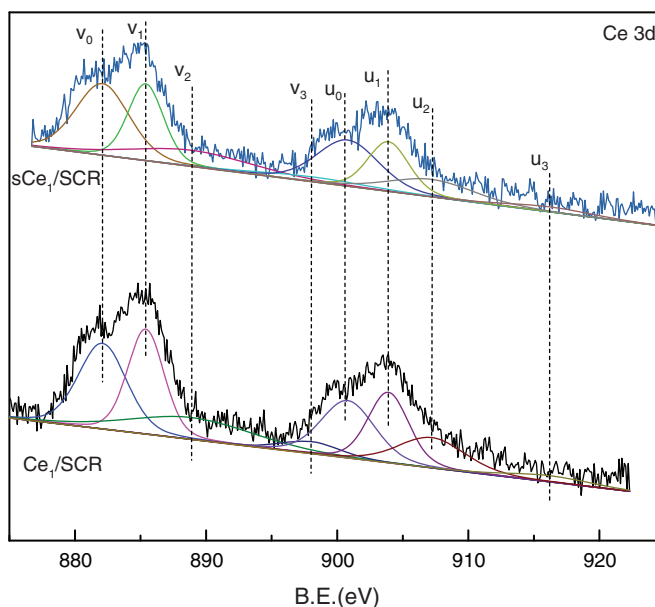
Figure 11: Ce3d XPS spectra for Ce_1/SCR and Ce_1/SCR
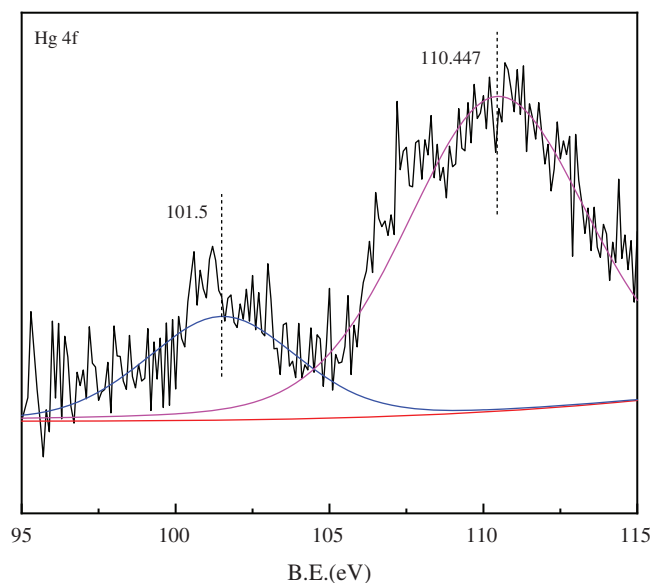
Figure 12: Hg4f XPS spectra for sCe_1/SCR

5.3 Mechanism

Previous studies have shown that the interconversion of V^{4+}/V^{5+} participates in the reaction process of Hg^0 catalytic oxidation over SCR. Based on the results above, a possible mechanism for Hg^0 oxidation can be proposed as follows:

$$2HCl(g) + V_2O_5 = 2Cl^*(ad) + V_2O_4 + H_2O \tag{8}$$

$$2Cl(ad) + Hg^0(g) = HgCl_2(g) \tag{9}$$

$$V_2O_4 + 2CeO_2 = V_2O_5 + Ce_2O_3 \tag{10}$$

$$2Ce_2O_3 + O_2 = 4CeO_2 \tag{11}$$

HCl was adsorbed onto the active sites of catalyst and reacted with chemisorbed oxygen from V_2O_5 to form active surface chlorine species, which then would react with gas-phase or weakly bonded Hg^0 to produce $HgCl_2$. The redox process of V^{4+}/V^{5+} was contributed by the shift of CeO_2/Ce_2O_3. The missing lattice oxygen of CeO_2 would be replaced by O_2. The redox cycle ($V^{4+} + Ce^{4+} \leftrightarrow V^{5+} + Ce^{3+}$) played an important role in promoting Hg^0 oxidation.

6 Conclusion

Ce doping can significantly improve the catalytic activity for Hg^0 oxidation of SCR catalyst Ce_1/SCR (1%Ce, wt.%) displayed the best performance with an Hg^0 oxidation efficiency of 21.2% higher than that of SCR catalyst in simulated coal-fired flue gas at 350°C. Ce_1/SCR also enhanced NO conversion efficiency at 200–400°C. H_2O in flue gas had an inhibitive effect on Hg^0 oxidation. However, Ce_1/SCR showed a better H_2O resistance but a slightly weaker SO_2 resistance than SCR catalyst. NO had a slight promotion effect on the Hg^0 oxidation over Ce_1/SCR. The XPS results indicated that Ce_1/SCR possed more chemisorbed oxygen and better redox ability compared with SCR catalyst. The catalytic mechanism was that adsorbed HCl was oxidized by chemisorbed oxygen to form active chlorine which would react with gas-phase or weakly bonded Hg^0 to form $HgCl_2$. HCl played an essential role in Hg^0 oxidation, and the redox cycle ($V^{4+} + Ce^{4+} \leftrightarrow V^{5+} + Ce^{3+}$) had an important role in promoting Hg^0 oxidation.

Conflicts of Interest: The authors declare that they have no conflicts of interest to report regarding the present study.

References

1. Pacyna, J. M., Travnikov, O., de Simone, F., Hedgecock, I. M., Sundseth, K. et al. (2016). Current and future levels of mercury atmospheric pollution on a global scale. *Atmospheric Chemistry and Physics, 16(19),* 12495–12511. DOI 10.5194/acp-16-12495-2016.

2. Vidic, R. D., McLaughlin, J. B. (1996). Uptake of elemental mercury vapors by activated carbons. *Journal of the Air & Waste Management Association, 46(3),* 241–250. DOI 10.1080/10473289.1996.10467458.

3. Ren, J., Zhou, J., Luo, Z., Cen, K. (2002). Study of mercury emission during coal combustion. *Acta Scientiae Circumstantiae, 22(3),* 289–293. DOI 10.13671/j.hjkxxb.2002.03.004.

4. Zhang, L., Wang, S., Wu, Q., Wang, F., Lin, C. et al. (2016). Mercury transformation and speciation in flue gases from anthropogenic emission sources: A critical review. *Atmospheric Chemistry and Physics, 16(4),* 2417–2433. DOI 10.5194/acp-16-2417-2016.

5. Wang, Y., Duan, Y., Yang, L., Meng, S., Wang, Q. (2008). Experimental study on mercury removed by combined wet-method flue gas desulphurization devices in combination with electrostatic precipitators. *Proceedings of China Electric Machinery Engineering, 28(29),* 64–69. DOI 10.13334/j.0258-8013.pcsee.2008.29.003.

6. Yin, L., Zhuo, Y., Xu, Q., Zhu, Z., Du, W. et al. (2013). Mercury emission from coal-fired power plants in China. *Proceedings of the CSEE, 33(29),* 1–10. DOI 10.13334/j.0258-8013.pcsee.2013.29.004.

7. Xu, W., Wang, J., Wang, W. (2010). Exploratory study of mercury removal effectiveness in various morphology and states during the dust removal and desulphurization treatment of coalfired flue gases. *East China Electric Power, 38(1),* 47–50. DOI CNKI:SUN:HDDL.0.2010-01-016.

8. Yan, R., Liang, D. T., Tay, J. H. (2003). Control of mercury vapor emissions from combustion flue gas. *Environmental Science and Pollution Research, 10(6),* 399–407. DOI 10.1065/espr2003.04.149.

9. Chen, J., Yuan, D., Li, Q., Zheng, J., Zhu, Y. et al. (2008). Effect of flue-gas cleaning devices on mercury emission from coal-fired boiler. *Proceedings of the CSEE, 28(2),* 72–76. DOI 10.13334/j.0258-8013.pcsee.2008.02.012.

10. Reddy, B. M., Khan, A., Yamada, Y., Kobayashi, T., Loridant, S. et al. (2003). Structural characterization of CeO_2-TiO_2 and V_2O_5/CeO_2-TiO_2 catalysts by Raman and XPS techniques. *Journal of Physical Chemistry B, 107(22),* 5162–5167. DOI 10.1021/jp0344601.

11. Chi, G., Shen, B., Zhu, S., Chuan, H. (2016). Oxidation of elemental mercury over modified SCR catalysts. *Journal of Fuel Chemistry and Technology, 44(6),* 763–768. DOI 10.3969/j.issn.0253-2409.2016.06.018.

12. Zhao, L., Li, C., Zhang, J., Zhang, X., Zhan, F. et al. (2015). Promotional effect of CeO_2 modified support on V_2O_5-WO_3/TiO_2 catalyst for elemental mercury oxidation in simulated coal-fired flue gas. *Fuel, 153,* 361–369. DOI 10.1016/j.fuel.2015.03.001.

13. Chi, G., Shen, B., Yu, R., He, C., Zhang, X. (2017). Simultaneous removal of NO and Hg^0 over Ce-cu modified V_2O_5/TiO_2 based commercial SCR catalysts. *Journal of Hazardous Materials, 330,* 83–92. DOI 10.1016/j.jhazmat.2017.02.013.

14. Zhao, L., He, Q. S., Li, L., Lu, Q., Dong, C. Q. et al. (2015). Research on the catalytic oxidation of Hg^0 by modified SCR catalysts. *Journal of Fuel Chemistry and Technology, 43(5),* 628–634. DOI 10.1016/S1872-5813(15)30018-9.

15. Li, H., Wu, C., Li, Y., Zhang, J. (2011). CeO_2-TiO_2 catalysts for catalytic oxidation of elemental mercury in low-rank coal combustion flue Gas. *Environmental Science & Technology, 45(17),* 7394–7400. DOI 10.1021/es2007808.

16. Pang, C., Zhuo, Y., Weng, Q. (2017). Mn/SAPO-34 as an efficient catalyst for the low-temperature selective catalytic reduction of NO_x with NH_3. *RSC Advances, 7(51),* 32146–32154. DOI 10.1039/C7RA05165D.

17. Shan, W., Liu, F., He, H., Shi, X., Zhang, C. (2012). A superior Ce–W–Ti mixed oxide catalyst for the selective catalytic reduction of NOx with NH_3. *Applied Catalystis B: Environmental, 115,* 100–106. DOI 10.1016/j.apcatb.2011.12.019.

18. Fang, J., Bi, X., Si, D., Jiang, Z., Huang, W. (2007). Spectroscopic studies of interfacial structures of CeO_2–TiO_2 mixed oxides. *Applied Surface Science, 253(22),* 8952–8961. DOI 10.1016/j.apsusc.2007.05.013.

19. Wang, P., Su, S., Xiang, J., Cao, F., Sun, L. et al. (2013). Atalytic oxidation of Hg^0 by CuO–MnO_2–Fe_2O_3/–Al_2O_3 catalyst. *Chemical Engineering Journal, 225,* 68–75. DOI 10.1016/j.cej.2013.03.060.

20. He, H., Dai, H. X., Au, C. T. (2004). Defective structure, oxygen mobility, oxygen storage capacity, and redox properties of RE-based (RE = Ce, Pr) solid solutions. *Catalysis Today, 90(3–4),* 245–254. DOI 10.1016/j.cattod.2004.04.033.